Optimization and Uncertainty Analysis of Co-combustion Ratios in a Semi-Isolated Green Energy Combined Cooling, Heating, and Power System (SIGE-CCHP)

Jie Ji[a*], Wenchao Wen[a], Yingqi Xie[a], Aoyun Xia[a], Wenjie Wang[a], Jinbo Xie[a], Qingyuan Yin[a], Mengyu Ma[a], Hui Huang[a], Xiaolong Huang[a], Chu Zhang[a], Yaodong Wang[b]

[a]Huaiyin institute of technology, Huaiyin Jiangsu 223002, China

[b] Durham Energy Institute Durham University

Abstract: This study delved into the integration of biomass gas and natural gas within a Combined Cooling, Heating, and Power (CCHP) system. A Semi-Isolated Green Energy CCHP (SIGE-CCHP) model was devised to scrutinize the performance of co-firing equipment across diverse optimization objectives, while manipulating the proportions of natural gas and biomass gas as inputs. Findings revealed that escalating the share of biomass gas led to a reduction in carbon emissions but triggered an escalation in operational and maintenance costs. However, at an optimal mixing ratio of 1:1, carbon emissions exhibited marginal increments, coupled with a substantial decrease in operational and maintenance expenses. Notably, when prioritizing operational and maintenance costs, the system exhibited optimal performance, resulting in a notable 26.76% cost reduction. Conversely, when prioritizing carbon emissions, the system metamorphosed into a carbon sequestration entity, with a maximal capacity to absorb 2021.86kg of carbon dioxide. This study furnishes theoretical underpinnings for optimizing the operation of co-firing equipment, augmented by a sensitivity analysis aimed at intuitively elucidating the repercussions of varying mixing ratios on the system.

Keywords: SIGE-CCHP; biomass gas; mixed burning of natural gas; operation and maintenance costs; carbon emissions; sensitivity analysis

Introduction

The relentless advancement of the economy invariably accompanies heightened energy consumption, precipitating substantial carbon emissions from diverse production capacities. In response, China has articulated the strategy of attaining carbon peak and eventual carbon neutrality, catalyzing a profound transformation within the energy industry. This strategic imperative has prompted multifaceted efforts aimed at curtailing carbon emissions, thereby positioning it as a pivotal focal point for future research endeavors. Wind energy, solar energy, and biomass have emerged as focal points for intensive investigation, embodying pivotal avenues for advancing carbon reduction initiatives within the energy landscape [1].

The intrinsic renewable characteristics of biomass render it indispensable in energy frameworks, particularly within Combined Cooling, Heating, and Power (CCHP) systems. Reference [2] proposes an integrated CCHP system combining biomass, natural gas, and geothermal energy. It offers a promising approach for renewable energy and fossil fuel integration in rural China, enhancing energy efficiency and addressing environmental challenges. Reference [3] establishes a bidirectional relationship between system capacity and operation strategy in renewable CCHP systems. It proposes an optimization method for primary energy savings, cost reduction, and CO_2 emission mitigation. Reference [4] presents a biomass-based CCHP model with gasification, fuel cells, engine generators, and absorption refrigeration. Parametric analysis

Corresponding Author E-mail Address: jijie@hyit.edu.cn

demonstrates the importance of optimizing steam-to-biomass ratio and fuel utilization for improved electrical efficiency. However, the reliability and stability of biomass supply pose significant challenges. Given the seasonal and geographical constraints associated with biomass resources, supply instability may compromise system continuity and energy supply reliability. To address this, the proposed system architecture allows for seamless integration with external energy systems, thereby facilitating energy sharing and exchange.

Reference [5] examined steam injection into a biomass-based cogeneration system, finding that injection into the vaporizer increased efficiency by 5.43% and reduced CO2 emissions by 5.2%. Reference [6] introduced a sustainable power system using biomass, promoting clean production and energy independence. Advances in battery technology [7, 8] have facilitated energy storage in CCHP systems [9]. Reference [10] presented a modeling method for biomass-based CCHP systems, achieving cost savings and high energy efficiency. Reference [11] conducted a lifecycle assessment of biomass CCHP systems, enhancing energy efficiency and reducing production costs. Reference [12] proposed a biomass-integrated CCHP system achieving renewable energy contributions of 72.11%. Reference [13] designed an efficient household CCHP system, reducing costs and CO_2 emissions. Reference [14] optimized a hybrid power system for CCHP, reducing annual costs. The intricacies inherent in biomass, coupled with the uncertainties surrounding its procurement, imbue the system with complexity, necessitating the formulation of system designs and control strategies tailored to the unique characteristics of biomass. Furthermore, challenges persist in the processing and conversion of biomass, encompassing issues related to technological feasibility and the scalability of applications. Many biomass processing technologies remain in the nascent stages of research and experimentation, lacking the maturity requisite for widespread commercial implementation. The architectural framework posited within this study offers the prospect of integration with external energy systems, thereby fostering the judicious exploitation of energy reservoirs.

Reference [15] investigated the optimization of a biomass gasification CCHP system with a ground source heat pump, demonstrating improvements in cost savings, energy efficiency, carbon emissions, and overall performance. Reference [16] introduced a residential CCHP system incorporating a biomass gasifier, fuel cell stack, absorption chiller, and auxiliary equipment, effectively reducing carbon emissions. Reference [17] presented an innovative solid oxide fuel cell CCHP system integrated with biomass gasification, offering various waste heat modes for optimal performance. Reference [18] proposed a net zero-emission CCHP system for dimethyl ether production using biomass gasification, resulting in reduced CO_2 emissions and cost savings. Reference [19] integrated four subsystems to create a power generation system utilizing syngas from biomass gasification, demonstrating technical feasibility, economic benefits, and environmental soundness. The combustion of biomass presents an environmental challenge due to the emission of gases and particulate matter. While biomass combustion yields lower carbon emissions compared to fossil fuels, it still releases harmful substances and particulates, thereby posing potential threats to air quality and human health. Furthermore, the processing and conversion of biomass may entail substantial water, energy, and resource consumption, thereby presenting obstacles to sustainable development and resource efficiency. The proposed system architecture in this study offers connectivity to external energy systems, effectively addressing the environmental concerns associated with energy utilization processes.

Reference [20] presents a system employing biomass carbon dioxide gasification, carbon

Corresponding Author E-mail Address: jijie@hyit.edu.cn

capture solid oxide fuel cells, and organic Rankine cycles, demonstrating its efficacy in reducing carbon emissions. Reference [21] introduces a biomass gasification device utilizing carbon dioxide as a gasification agent to minimize emissions and enhance energy efficiency. Exergy analysis of the process identifies substantial irreversibility losses in the gasification and burner units, highlighting the importance of regular equipment maintenance. Reference [22] compares the performance of micro gas turbine and supercritical carbon dioxide systems, both fueled by biomass gasifiers and yielding similar nominal net power output. Results show the supercritical system's significantly higher net thermal power output, leading to enhanced overall efficiency. Reference [23] evaluates a biomass gasification-based CCHP system, showcasing its provision of sustainable and eco-friendly cooling and power solutions for data centers. Reference [24] analyzes an innovative biomass gasification-based CCHP system for power generation, revealing tar pollution challenges necessitating complex gas purification devices for syngas used in the internal combustion engine. This aspect is pivotal for assessing system feasibility and sustainability. Lastly, Reference [25] investigates the integration of a Stirling engine in a gasification-based CCHP system to mitigate tar pollution. Existing literature highlights inefficiencies in current CCHP systems, particularly regarding energy utilization. This paper proposes a novel framework aimed at enhancing energy efficiency through improved interconnectivity among energy systems. Operational costs of existing CCHP systems are notably high, primarily attributed to energy procurement and equipment maintenance expenses. However, the proposed framework facilitates energy sharing and exchange with external systems, thereby mitigating procurement costs. The construction and integration of conventional CCHP systems entail complex coordination among multiple energy devices and systems, presenting significant integration challenges. In contrast, the proposed framework effectively integrates the CCHP system with external energy systems, reducing the complexity of integrating multiple devices and systems and streamlining construction and operation processes. Moreover, current CCHP systems exhibit limited flexibility and scalability, hindering adjustment and expansion according to evolving needs. In contrast, the proposed framework offers customizable design and layout options, better aligning with user requirements and offering scalability potential. Hence, operational and maintenance costs emerge as critical considerations in biomass gasification systems.

Reference [26] discusses the development of an integrated CCHP (Combined Cooling, Heating, and Power) system tailored for biomass and natural gas co-combustion. The study primarily investigates exergy production and thermodynamic efficiency. In a similar vein, Reference [27] proposes a CCHP system integrated with a ground source heat pump, utilizing a blend of biomass gas and natural gas for combustion. Through modeling, the study evaluates exergy and exergy economy, exploring system performance across varying mixing ratios. Additionally, Reference [28] presents a dual-fuel CCHP system, amalgamating multiple components to assess thermodynamic and exergy economic performances, particularly during summer and winter conditions. Existing research often falls short in conducting comprehensive investigations into flexible hybrid ratio systems across diverse application scenarios. Different scenarios exhibit unique energy demand profiles and operational modes, yet current literature often overlooks these practical considerations. Flexible hybrid ratio systems represent intricate energy frameworks necessitating coordinated operation among multiple input and output components. However, scholarly inquiry lacks systematic analyses of their operational characteristics and the influence of various factors on performance. Despite the potential of

Corresponding Author E-mail Address: jijie@hyit.edu.cn

flexible hybrid ratio systems in enhancing energy efficiency and environmental sustainability, their full capabilities remain underexplored in existing research. Furthermore, the stability and reliability of these systems are paramount for practical implementation, yet scholarly exploration into these aspects remains limited. Although some studies have addressed biomass exergy and thermal economy, they have neglected crucial aspects such as carbon emissions and operation and maintenance (O&M) costs associated with the combined combustion of natural gas and biomass. Future research should investigate carbon emissions across different combustion ratios and consider O&M requirements for co-firing, thus advancing our understanding of flexible hybrid ratio systems.

Several studies have addressed the integration of carbon emissions and economic considerations in the operation of IES systems. References [29] and [30] aim to minimize operating costs and pollutant emissions, while [31] emphasizes the economic and environmental aspects. Reference [32] focuses on minimizing energy costs and reducing carbon dioxide emissions in a CCHP-PV system. Similarly, [33] aims to minimize system operation costs and carbon emission expenses in a P2G-CCHP system. Reference [34] considers cost savings, energy conservation, and emission reduction as objectives, and [35] explores multi-objective optimization for minimizing energy costs and emissions in residential microgrids. Existing research often oversimplifies complex performance regulation in energy systems, overlooking intricate interactions and dependencies. This paper addresses this oversight by examining multiple energy inputs, outputs, and conversion processes, beyond a single optimization problem. With growing global concern over carbon emissions, there's a need for deeper analysis and strategies to reduce emissions in energy systems. However, current research lacks comprehensive analysis and systematic study in this area. Additionally, prevailing economic analyses often lack depth, focusing mainly on simplistic cost-benefit comparisons. Optimization methods also suffer from limitations in addressing uncertainties and dynamic characteristics of energy systems. This study integrates economic and carbon emission objectives to explore system performance comprehensively, filling gaps in current research methodologies.

Building upon the aforementioned research, this study takes a comprehensive approach by examining the co-combustion of natural gas and biomass gas in varying proportions. It compares different optimization objectives to analyze the system's performance, carbon emissions, and operational and maintenance costs. By conducting this analysis, the paper aims to contribute to the scholarly literature with a more rigorous and academic writing style, enhancing its language proficiency and adherence to top-tier journal standards.

1 1SIGE-CCHP system operation framework

The Integrated Energy System (IES) employs a diverse array of energy sources and equipment to meet the internal demand of the system. Building upon an established model (reference [36]), this study introduces the co-combustion of natural gas and biomass gas at varying mixing ratios. It investigates how different optimization objectives influence the system, selecting various targets for comparison during the solution process. The specific framework is depicted in Fig.1.

As illustrated in Fig.1, the IES model comprises several key components, including the Mixer-Heat Exchanger (MXHE), Wind Turbine (WT), Photovoltaic System (PV), Gas Turbine (GT), Electric Chiller (EC), Electrolysis Hydrogen Generation Equipment (EL), Methane Generator (MR), Hydrogen Fuel Cell (HFC), Waste Heat Recovery Boiler (WHRB), Heat

Corresponding Author E-mail Address: jijie@hyit.edu.cn

Exchanger (HEX), Gas Boiler (GB), and Steam Double-Effect Lithium Bromide Absorption Chiller (AC.W). Energy storage is facilitated by the Battery (SB), Thermal Storage Tank (HST), Cold Storage Tank (CST), Natural Gas Storage Tank (NGST), and Hydrogen Storage Tank (H2ST).

Within the system, the electric load is managed through coordinated provision from wind power, photovoltaic sources, and gas turbines. Additionally, electricity can be procured from the distribution network during periods of insufficient power supply. The heat load is primarily sustained by gas turbines and gas boilers, while the cooling load is met by a steam double-effect lithium bromide absorption chiller and an electric refrigerator. Equipment parameters are detailed in Tables 1-3, referencing the specifications outlined in reference [36].

Table 1 Equipment parameters

equipment	Capacity / kW	Energy conversion efficiency / %	Climbing constraint / %
GT	400	0.35	20%
GB	300	0.9	20%
EL	500	0.87	20%
MR	250	0.6	20%
HFC	250	0.85	20%
WHRB	/	0.85	20%
HEX	/	0.8	20%
AC.W	/	1.31	20%

Table 2 Energy storage parameters

energy storage device	Capacity / kW	Capacity lower bound constraint / %	Capacity upper limit constraint / %	Climbing constraint / %
Electric	450	10	90	20
Heat	500	10	90	20
Cool	150	10	90	20
H_2	200	10	90	20
Natural	150	10	90	20

Table 3 Parameters of actual carbon emission model

Power consumption type			**Natural gas consumption type**		
a_1	b_1	c_1	a_2	b_2	c_2
36	-0.38	0.0034	3	-0.004	0.001

Corresponding Author E-mail Address: jijie@hyit.edu.cn

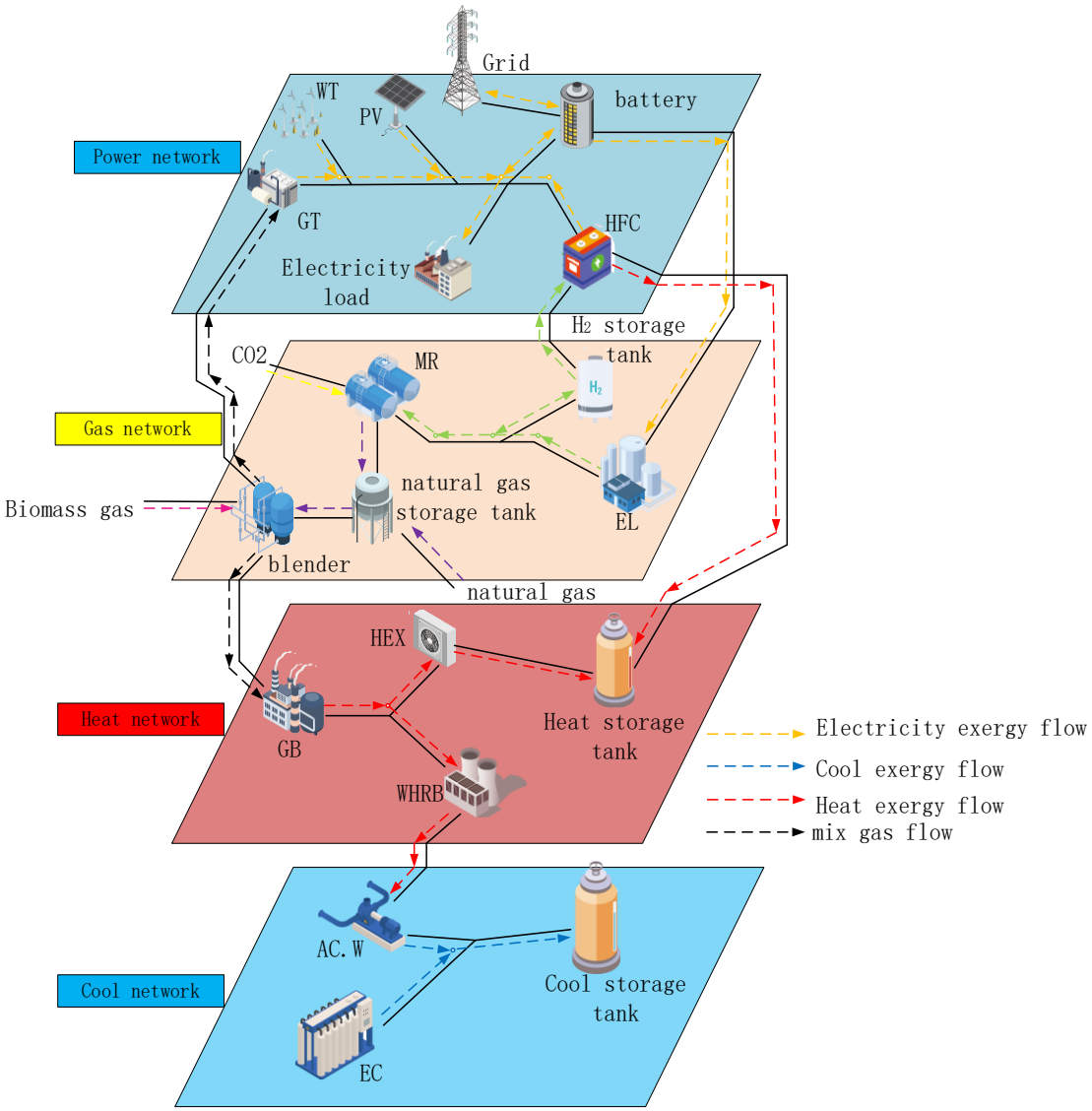

Fig.1 Structure of SIGE-CCHP system

1.1 Gas turbine model

The gas turbine serves as a crucial piece of research equipment within this system. Formula (1) provides insights into the fuel consumption power of the gas turbine across various mixing ratios.

$$\begin{cases} P_{GT,e}(t) = \eta_{GT}^{e} P_{GT,mg}(t) \\ P_{GT,h}(t) = \eta_{GT}^{h} P_{GT,mg}(t) \\ P_{GT,mg}^{\min} \le P_{GT,mg}(t) \le P_{GT,mg}^{\max} \\ \Delta P_{GT,mg}^{\min} \le \left| P_{GT,mg}(t+1) - P_{GT,mg}(t) \right| \le \Delta P_{GT,mg}^{\max} \end{cases} \tag{1}$$

In the formula, $P_{GT,mg}(t)$ designates the mixed gas power of natural gas and biomass gas input into the gas turbine (GT) during the time period t. $P_{GT,e}(t)$ and $P_{GT,h}(t)$ correspond to

Corresponding Author E-mail Address: jijie@hyit.edu.cn

the electrical and thermal energy outputs of the GT during the same time period, respectively. η_{GT}^{e} and η_{GT}^{h} represent the efficiencies of the GT in converting the mixed gas into electrical and thermal energy, respectively. $P_{GT,mg}^{\max}$ and $P_{GT,mg}^{\min}$ represent the upper and lower bounds for the mixed gas power input into the GT, whereas $\Delta P_{GT,mg}^{\max}$ and $\Delta P_{GT,mg}^{\min}$ designate the upper and lower limits for the combined heat and power (CHP) ramp-up, respectively.

1.2 Gas-fired boiler model

The gas boiler functions as supplementary research equipment within the system, employing mixed gas with diverse mixing ratios as its fuel source. Its power consumption can be consulted in formula (2).

$$\begin{cases} P_{GB,h}(t) = \eta_{GB}^{h} P_{GB,mg}(t) \\ P_{GB,mg}^{\min} \le P_{GB,mg}(t) \le P_{GB,mg}^{\max} \\ \Delta P_{GB,mg}^{\min} \le \left| P_{GB,mg}(t+1) - P_{GB,mg}(t) \right| \le \Delta P_{GB,mg}^{\max} \end{cases} \tag{2}$$

In the formula, $P_{GB,mg}(t)$ represents the power of the mixed gas of natural gas and biomass gas input into the gas turbine (GB) during the period t; $P_{GB,h}(t)$ represents the heat energy output of the gas turbine (GB) during the period t; η_{GB}^{h} indicates the efficiency of the gas turbine (GB) in converting the mixed gas into heat energy; $P_{GB,mg}^{\max}$ and $P_{GB,mg}^{\min}$ represent the upper and lower limits of the mixed gas power input into the gas turbine (GB), respectively; while $\Delta P_{GB,mg}^{\max}$ and $\Delta P_{GB,mg}^{\min}$ represent the upper and lower limits of the combined heat and power (CHP) ramp-up of the gas turbine (GB), respectively.

1.3 Two-stage operation process of P2G

According to the literature [36], hydrogen energy, being an efficient and clean energy source, exhibits excellent compatibility with hydrogen fuel cells.

1) EL equipment.

$$\begin{cases} P_{EL,h2}(t) = \eta_{EL} P_{EL,e}(t) \\ P_{EL,e}^{\min} \le P_{EL,e}(t) \le P_{EL,e}^{\max} \\ \Delta P_{EL,e}^{\min} \le \left| P_{EL,e}(t+1) - P_{EL,e}(t) \right| \le \Delta P_{EL,e}^{\max} \end{cases} \tag{3}$$

Where $P_{EL,e}(t)$ signifies the electric energy input to EL during the t period; $P_{EL,h2}(t)$ denotes the output hydrogen energy; η_{EL} represents the energy conversion efficiency of EL; $P_{EL,e}^{\max}$ and $P_{EL,e}^{\min}$ indicate the upper and lower boundaries for the electric energy input to EL,

Corresponding Author E-mail Address: jijie@hyit.edu.cn

respectively; $\Delta P_{EL,e}^{\max}$ and $\Delta P_{EL,e}^{\min}$ and G depict the respective upper and lower climbing limits of EL.

2) MR equipment.

$$\begin{cases} P_{MR,g}(t) = \eta_{MR} P_{MR,h2}(t) \\ P_{MR,h2}^{\min} \le P_{MR,h2}(t) \le P_{MR,h2}^{\max} \\ \Delta P_{MR,h2}^{\min} \le \left| P_{MR,h2}(t+1) - P_{MR,h2}(t) \right| \le \Delta P_{MR,h2}^{\max} \end{cases} \tag{4}$$

Where $P_{MR,h2}(t)$ denotes the hydrogen energy inputted into MR during the t period, $P_{MR,g}(t)$ represents the natural gas power outputted by MR in the same time frame, η_{MR} signifies the energy conversion efficiency of MR, $P_{MR,h2}^{\max}$ and $P_{MR,h2}^{\min}$ establish the respective upper and lower bounds for the hydrogen energy input into MR, $\Delta P_{MR,h2}^{\max}$ and $\Delta P_{MR,h2}^{\min}$ delineate the maximum and minimum climbing limits of MR, respectively.

3) HFC equipment.

HFC utilizes hydrogen as its principal fuel, enabling consistent conversion of electrical and thermal energy. As a result, the following outlines the process of constructing the HFC model:

$$\begin{cases} P_{HFC,e}(t) = \eta_{HFC}^{e} P_{HFC,h2}(t) \\ P_{HFC,h}(t) = \eta_{HFC}^{h} P_{HFC,h2}(t) \\ P_{HFC,h2}^{\min} \le P_{HFC,h2}(t) \le P_{HFC,h2}^{\max} \\ \Delta P_{HFC,h2}^{\min} \le \left| P_{HFC,h2}(t+1) - P_{HFC,h2}(t) \right| \le \Delta P_{HFC,h2}^{\max} \end{cases} \tag{5}$$

Where $P_{HFC,h2}(t)$ denotes the hydrogen energy input to HFC in period t; $P_{HFC,e}(t)$ and $P_{HFC,h}(t)$ respectively signify the electrical and thermal energy outputs generated by HFC in period t; η_{HFC}^{e} and η_{HFC}^{h} respectively represent the conversion efficiencies of HFC corresponding to electrical and thermal energy; $P_{HFC,h2}^{\max}$ and $P_{HFC,h2}^{\min}$ respectively represent the upper and lower bounds of hydrogen energy input to HFC; $\Delta P_{HFC,h2}^{\max}$ and $\Delta P_{HFC,h2}^{\min}$ indicate the respective upper and lower limits of the climbing capability of HFC.

1.4 Heat recovery device

The heat recovery device primarily consists of a waste heat recovery boiler and a heat exchanger. These components efficiently capture the heat energy expelled by the gas turbine. The energy conversion process is outlined in Equation (6).

Corresponding Author E-mail Address: jijie@hyit.edu.cn

$$\begin{cases} P_{re,h}(t) = \lambda_1 \eta_{re}^{h} P_{GT,h}(t) \\ P_{HEX,h}(t) = \lambda_2 \eta_{HEX}^{h} P_{GT,h}(t) \end{cases} \tag{6}$$

Where $P_{GT,h}(t)$ represents the heat energy output by the gas turbine (GT) in period t; $P_{re,h}(t)$ denotes the heat energy output generated by the waste heat boiler in period t; η_{re}^{h} signifies the efficiency of heat energy conversion in the waste heat recovery boiler; $P_{HEX,h}(t)$ indicates the heat energy output from the heat exchanger during period t; η_{HEX}^{h} stands for the efficiency of the heat transfer device in converting heat energy; λ_1 represents the shunt parameter for the heat energy output of the GT, which is set at 0.8 in this context; λ_2 represents the shunt parameter for the thermal energy output of the GT, which is set at 0.2.

1.5 Steam double-effect lithium bromide absorption chiller

The conversion model pertaining to the output cooling capacity of the steam double-effect lithium bromide absorption chiller is formulated in Equation (7).

$$P_{AC,l}(t) = \mathrm{COP}_{AC}^{l} P_{re,h}(t) \tag{7}$$

Where $P_{AC,l}(t)$ represents the cold energy output of the steam double-effect lithium bromide absorption chiller during the t-period; COP_{AC}^{l} signifies the coefficient of performance for refrigeration in the steam double-effect lithium bromide absorption chiller.

1.6 Electric refrigerator

The refrigeration characteristics of the electric refrigerator are intricately linked to the refrigeration coefficient of the equipment, and the quantification of its output cooling capacity can be accurately captured through Formula (8).

$$\begin{cases} P_{EC,l}(t) = P_{EC,e}(t) \cdot COP_{EC,l} \\ P_{EC,e}^{\min} \le P_{EC,e}(t) \le P_{EC,e}^{\max} \\ \Delta P_{EC,e}^{\min} \le \left| P_{EC,e}(t+1) - P_{EC,e}(t) \right| \le \Delta P_{EC,e}^{\max} \end{cases} \tag{8}$$

Where $P_{EC,e}(t)$ denotes the electricity consumed by the electric chiller during the t-period; $P_{EC,l}(t)$ represents the cold energy generated by the electric chiller within the same time frame; $COP_{EC,l}$ signifies the coefficient of performance for refrigeration in the electric chiller; $P_{EC,e}^{\max}$ and $P_{EC,e}^{\min}$ designate the respective upper and lower bounds for the hydrogen energy input into the hydrogen fuel cell (HFC); $\Delta P_{EC,e}^{\max}$ and $\Delta P_{EC,e}^{\min}$ correspond to the upper and lower climbing

Corresponding Author E-mail Address: jijie@hyit.edu.cn

limits exhibited by the HFC.

1.7 Carbon emission model

The primary sources of carbon emissions within the Integrated Energy System (IES) encompass electricity procurement, gas turbines, and gas boilers.

The methane generator serves as the primary source of emission reduction. Consequently, its carbon emission model is formulated in Equation (9). [36].

$$\begin{cases} E_{IES} = E_{buy,e} + E_{all} - E_{MR} \\ E_{buy,e} = \sum_{t=1}^{T} (a_1 + b_1 P_{buy,e}(t) + c_1 P_{buy,e}^2(t)) \\ E_{all} = \sum_{t=1}^{T} (a_2 + b_2 P_{all}(t) + c_2 P_{all}^2(t)) \\ P_{all}(t) = P_{GT,e}(t) + P_{GB,h}(t) + P_{GT,h}(t) \\ E_{MR} = \sum_{t=1}^{T} \varphi P_{MR,g}(t) \end{cases} \tag{9}$$

Where E_{IES} denotes the Integrated Energy System (IES); E_{all1} represents the carbon emissions associated with electrical equipment; E_{all2} signifies the carbon emissions resulting from natural gas utilization; E_{all1} represents the actual carbon emissions of gas turbine, gas boiler and methane generator; E_{all2} represents the actual carbon emissions of electric refrigerators and power purchase; E_{MR} represents the actual amount of carbon dioxide absorbed by the methane generator; $P_{all1}(t)$ represents the equivalent output power of gas turbine, gas boiler and methane generator in t period; $P_{all2}(t)$ represents the equivalent output power of electric refrigerator and power purchase in t period; $P_{buy,e}(t)$ represents the power of electricity purchase in t period; a_1, b_1, c_1 and a_2, b_2, c_2 serve as carbon emission calculation parameters for electricity-consuming and gas-consuming energy supply equipment, respectively; φ represents the parameter of carbon dioxide absorption in the process of hydrogen energy conversion to natural gas in MR equipment.

2 SIGE-CCHP system operation model

2.1 Objective function

The SIGE-CCHP system introduced in this paper comprehensively incorporates the energy purchase cost, maintenance cost, carbon emissions, wind curtailment cost, and light curtailment cost associated with the Integrated Energy System (IES). Tailored to the distinct objectives of the three distinct scenarios, the following objective functions are established:

Corresponding Author E-mail Address: jijie@hyit.edu.cn

$$\begin{cases} F_1 = \min(F_2 + F_3) \\ F_2 = \min(f_{buy} + f_{mt} + f_{PV,\cos t} + f_{WT,\cos t}) \\ F_3 = \min(f_C) \end{cases} \tag{10}$$

Where F_1 represents the objective function for Scenario 1; F_2 represents the objective function for Scenario 2; F_3 represents the objective function for Scenario 3; f_{buy} stands for energy purchase cost; f_{mt} represents maintenance cost; f_C denotes carbon emissions; $f_{WT,\cos t}$ signifies wind curtailment cost; $f_{PV,\cos t}$ indicates light curtailment cost.

1) Cost A f_{buy}

$$f_{buy} = \sum_{t=1}^{T} \alpha_t P_{buy,e}(t) + \beta_t P_{buy,g}(t) \tag{11}$$

Where $P_{buy,e}(t)$ represents the power purchased during the time period t for electricity; $P_{buy,g}(t)$ represents the power purchased during the time period t for gas; α_t and β_t denote the purchase prices of electricity and gas, respectively, during the time period t.

2) Maintenance cost f_{mt}

$$\begin{cases} f_{mt} = \zeta_1 P_{GT,e}(t) + \zeta_4 P_{GB,e}(t) + \zeta_2 (P_{EL,e}(t) + P_{MR,g}(t) + P_{HFC,e}(t)) + \\ \qquad \zeta_3 P_{EC,e}(t) \end{cases} \tag{12}$$

Where ζ_1 represents the operation and maintenance cost coefficient for the gas turbine; ζ_2 denotes the operation and maintenance cost coefficient for the electrolysis hydrogen plant, methane generator, and hydrogen fuel cell, collectively referred to as; ζ_3 represents the operation and maintenance cost coefficient for the electric chiller, designated as; ζ_4 represents the operation and maintenance cost coefficient for the gas boiler, labeled as.

The relationship between ζ_1 and ζ_4 is specified in equation (13).

$$\zeta_1,\ \zeta_4 = \begin{cases} 0.05 \ ,0.35 & \text{n=0} \\ 0.075 \ ,0.4 & \text{n=1/4} \\ 0.1 \ ,0.45 & \text{n=2/4} \\ 0.125 \ ,0.5 & \text{n=3/4} \\ 0.15 \ ,0.55 & \text{n=4/4} \end{cases} \tag{13}$$

Corresponding Author E-mail Address: jijie@hyit.edu.cn

Where n represent the mixing ratio of natural gas and biomass gas.

3) Carbon emissions f_C

$$f_C = E_{IES} \tag{14}$$

4) Wind curtailment cost $f_{WT,\cos t}$

$$f_{WT,\cos t} = \theta_{WT,\cos t} \sum_{t=1}^{T} P_{WT,V}(t) - P_{WT,A}(t) \tag{15}$$

Where $\theta_{WT,\cos t}$ denotes the cost of wind curtailment per unit of power, measured in CNY per kilowatt (CNY/kW); $P_{WT,V}(t)$ and $P_{WT,A}(t)$ represent the expected and actual output power, respectively, during the time period t.

5) The cost of discarding light $f_{PV,cut}$

$$f_{PV,cut} = \theta_{PV,\cos t} \sum_{t=1}^{T} P_{PV,\mathrm{V}}(t) - P_{PV,A}(t) \tag{16}$$

Where $\theta_{PV,\cos t}$ denotes the cost of discarding light per unit of power, measured in CNY per kilowatt; $P_{PV,\mathrm{V}}(t)$ and $P_{PV,A}(t)$ represent the expected and actual output power, respectively, for the time period t.

2.2 Constraint conditions

1) Wind power output constraint

$$0 \le P_{WT}(t) \le P_{WT}^{\max} \tag{17}$$

Where $P_{WT}(t)$ denotes the wind power output during the t-th period; $P_{WT}^{\max}$ represents the upper limit of wind power output.

2) Photoelectric output constraint

$$0 \le P_{PV}(t) \le P_{PV}^{\max} \tag{18}$$

Where $P_{PV}(t)$ denotes the photoelectric output power during the t-th period; $P_{PV}^{\max}$ represents the upper limit of photoelectric output power.

3) GT, GB, EL, MR, HFC, electric refrigerator, operation constraints (see equations (1) to (5), (8)).

4) Energy storage operation constraints

In this paper, based on Reference [36], the energy storage equipment within the system serves primarily as a regulatory mechanism. Therefore, this paper uniformly models the electric, thermal, cooling, gas, and hydrogen energy storage equipment.

Corresponding Author E-mail Address: jijie@hyit.edu.cn

$$\begin{cases} 0 \le P_{ES,i}^{in}(t) \le B_{ES,i}^{in}(t) P_{ES,i}^{\max} \\ 0 \le P_{ES,i}^{out}(t) \le B_{ES,i}^{out}(t) P_{ES,i}^{\max} \\ P_{ES,i}(t) = \eta_{ES,i}^{in} P_{ES,i}^{in} - P_{ES,i}^{out} / \eta_{ES,i}^{out} \\ S_i(t) = S_i(t-1) + P_{ES,i}(t) / P_{ES,i}^{cap} \\ S_i(1) = S_i(T) \\ B_{ES,i}^{in}(t) + B_{ES,i}^{out}(t) = 1 \\ S_i^{\min} \le S_i(t) \le S_i^{\max} \end{cases} \tag{19}$$

Where $P_{ES,i}^{in}(t)$ and $P_{ES,i}^{out}(t)$ represent the charging and discharging power of the t period of the itch energy storage device respectively; $P_{ES,i}^{\max}$ represents the single charge and discharge maximum power of the itch energy storage device; both $B_{ES,i}^{in}(t)$ and $B_{ES,i}^{out}(t)$ represent binary variables, represents the charging and discharging state parameters of the itch energy storage device in t period, $B_{ES,i}^{in}(t)=1$ and $B_{ES,i}^{out}(t)=0$ represent the charging state; $B_{ES,i}^{in}(t)=0$ and $B_{ES,i}^{out}(t)=1$ represent the discharging state; $P_{ES,i}(t)$ represents the final output power of the I-type energy storage device in t period; $\eta_{ES,i}^{in}$ and $\eta_{ES,i}^{out}$ represent the charging and discharging efficiency of the itch energy storage device respectively; $S_i(t)$ represents the capacity of the second type of energy storage device in t period; $P_{ES,i}^{cap}$ represents the rated capacity of the itch energy storage device; $S_i^{\max}$ and $S_i^{\min}$ represent the upper and lower limits of the capacity of the itch energy storage device, respectively.

5) Electrical power balance

$$\begin{cases} P_{buy,e}(t) = P_{load,e}(t) + P_{EL,e}(t) + P_{EC,e}(t) + P_{ES}^{e}(t) - P_{WT}(t) - P_{PV}(t) - \\ \qquad P_{GT,e}(t) - P_{HFC,e}(t) \\ 0 \le P_{buy,e}(t) \le P_{buy,e}^{\max} \end{cases} \tag{20}$$

Where $P_{load,e}(t)$ denotes the electrical load during the t-th period; $P_{ES}^{e}(t)$ represents the input power of the electric storage in the t-th period; $P_{buy,e}^{\max}$ signifies the purchase limit of electricity for each time period.

6) Thermal power balance

$$P_{load,h}(t) + P_{ES}^{h}(t) = \mathrm{Q}_{HFC,h}(t) + \mathrm{Q}_{re,h}(t) + \mathrm{Q}_{HEX,h}(t) + \mathrm{Q}_{GB,h}(t) \tag{21}$$

Corresponding Author E-mail Address: jijie@hyit.edu.cn

Where $P_{load,h}(t)$ denotes the heat load during the t-th period, $P_{ES}^{h}(t)$ represents the power input to the heat storage in the t-th period.

7) Cold power balance

$$P_{load,l}(t)+P_{ES}^{l}(t)=Q_{EC,l}(t)+Q_{AC,l}(t) \tag{22}$$

Where $P_{load,l}(t)$ denotes the cooling load during the t-th period, $P_{ES}^{l}(t)$ represents the input power of the cold storage at time t.

8) Hydrogen power balance

$$P_{EL,h2}(t)=P_{MR,h2}(t)+P_{HFC,h2}(t)+P_{ES}^{h2}(t) \tag{23}$$

Where $P_{ES}^{h2}(t)$ represents the input power of hydrogen storage in t period.

9) Gas power balance

$$\begin{cases} P_{buy,g}(t)=\sigma P_{GT,mg}(t)+\sigma P_{GB,mg}(t)+P_{ES}^{g}(t)-P_{MR,g}(t) \\ 0\le P_{buy,g}(t)\le P_{buy,g}^{\max} \end{cases} \tag{24}$$

Where $P_{ES}^{g}(t)$ denotes the input power of natural gas storage during the t-th period; σ represents the proportion of natural gas; $P_{buy,g}(t)$ signifies the gas purchasing power at time t; $P_{buy,g}^{\max}$ indicates the gas purchase limit for each time period.

3 model solution.

In this paper, the flying ant algorithm is used to solve the proposed model.

The flying ant algorithm has the advantages of high precision, avoiding local ability and wide application field. Due to the addition of the accident rate η, the entire algorithm has a certain degree of randomness, reducing the situation of falling into local optimum. As the number of iterations increases, it quickly approaches the optimal value and accelerates the convergence speed. The accident rate η is as follows:

$$\eta=\frac{T-t}{T}\times e^{-\tan(\frac{t}{T}\times\frac{\pi}{2})}rand \tag{25}$$

When $\eta<0.5$, represents a safe arrival, change the formula as follows:

$$X_i(t+1)=X_i(t)+(w_1+\eta+\cos\theta)\left(\mathrm{X}_{best}-x_i(t)\right) \tag{26}$$

$$\theta=\frac{\mathrm{t}}{2\cdot\mathrm{T}}\cdot\pi \tag{27}$$

Where $X_i(t+1)$ represents the position of the next generation of flying ant I, and $X_i(t)$ represents the position of flying ant I at time t; w_1 represents the attraction of resource points.

Corresponding Author E-mail Address: jijie@hyit.edu.cn

$\cos\theta$ gradually approaching 0, the impact is getting smaller and smaller. X_{best} represents the position where the evaluation value is the largest, that is, the global optimal point.

When $0.5 \le \eta < 0.7$, represents an accident, but not dead, will fall in the vicinity.

$$X_i(t+1) = X_i(t) + \eta \times \text{rand} \tag{28}$$

Where η represents the accident rate, $X_i(t+1)$ represents the position of the next generation of flying ant I, $X_i(t)$ represents the position of flying ant I at time t, and $rand$ represents the random number from 0 to 1.

When $\eta \ge 0.7$, it represents the death in distress. At this time, a flying ant needs to be randomly supplemented in the area.

$$X_i(t+1) = lb + (ub - lb) \times rand \tag{29}$$

Where $X_i(t+1)$ represents the position of the next generation of flying ant I, lb represents the lower bound, ub represents the upper bound, and $rand$ represents the random number from 0 to 1.

The algorithm flow chart is shown in Fig.2;

4 Example analysis

In this study, the flying ant algorithm is employed to tackle the problem at hand, and various comparison cases are meticulously designed to comprehensively evaluate operational and maintenance costs, as well as carbon emissions. The empirical data collection endeavors were conducted within the SuBei Industrial Park. The research team has conducted preliminary fieldwork, yielding noteworthy findings, with some data already disseminated in reference[37]. The load data utilized in this investigation originates from the industrial park, encompassing enterprises with diverse demands for cold, heat, and power. These data are derived from firsthand research, ensuring the empirical integrity and precision of the study. Leveraging this robust dataset, the primary objective of this research is to conduct a thorough analysis and gain insights into the operational characteristics of the energy system within the industrial park. Ultimately, the study aims to furnish a scientific foundation for energy management and optimization endeavors.

In order to conduct a thorough comparative analysis of three different cases with varying mixing ratios, this study focuses on optimizing operation and maintenance costs and carbon emissions in Case 1, prioritizes operation and maintenance cost optimization in Case 2, and emphasizes carbon emissions optimization in Case 3. To facilitate this analysis, the study introduces energy storage parameters (Table 1), an actual emission model (Table 2), and equipment parameters (Table 3). The calculations are based on prevailing time-of-use electricity prices, as well as the prices of natural gas and biomass gas, while factoring in the impact of operation and maintenance costs and carbon emissions. Specifically, the price of natural gas is set at 0.35 CNY/ (kW ·h), and the price of biomass gas is 0.4 CNY/ (kW ·h). By employing the flying ant algorithm, the study calculates and analyzes five different mixing ratios: 1:0 (a), 0.75:0.25 (b),

Corresponding Author E-mail Address: jijie@hyit.edu.cn

0.5:0.5 (c), 0.25:0.75 (d), and 0:1 (e). This comprehensive approach allows for a deeper exploration of the effects of different cases and mixing ratios on operation and maintenance costs and carbon emissions, thereby offering a scientific foundation for informed decision-making. This revised description adheres to the writing style and scholarly standards expected by top-tier journals, enhancing language precision and academic rigor without altering the word count.

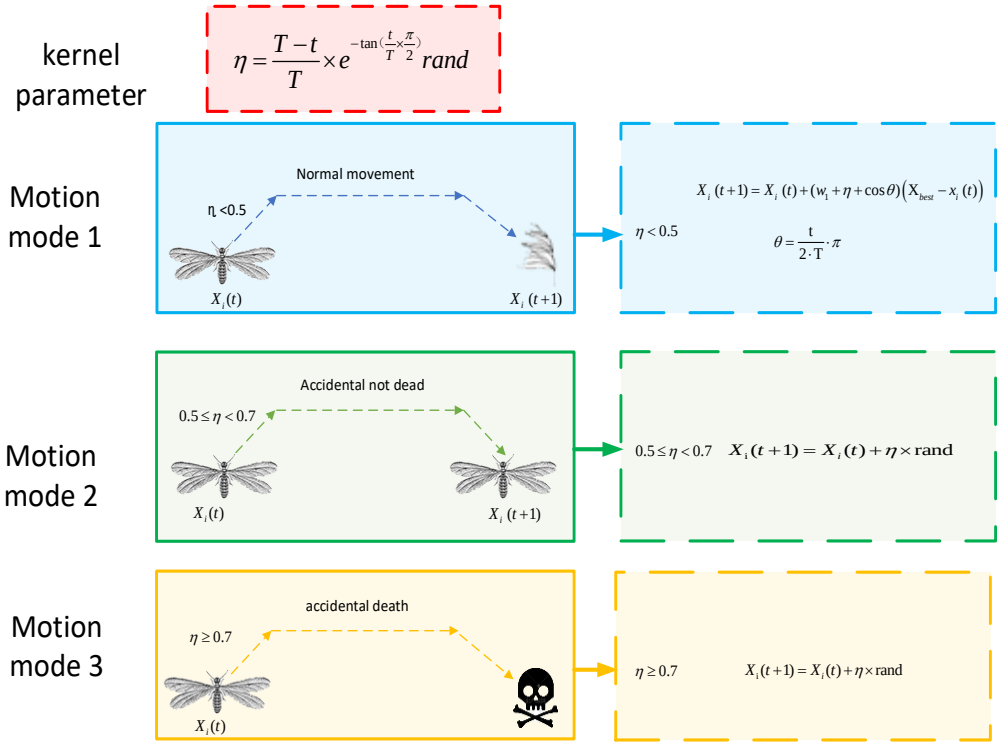

Fig.2 Algorithm details

4.1 Case analysis

In the following study of equipment output characteristics, the icons can be categorized into five different ratios: 1:0 (a), 0.75:0.25 (b), 0.5:0.5 (c), 0.25:0.75 (d), and 0:1 (e). These ratios represent the following mixtures: 100% natural gas (a), 75% natural gas and 25% biomass gas (b), 50% natural gas and 50% biomass gas (c), 25% natural gas and 75% biomass gas (d), and 100% biomass gas (e).

4.1.1 Comparative Analysis 1

From Fig.3 (a) and Table 4, it can be seen that compared with carbon emissions, the carbon emissions of Case 1 decreased by 9.69 % and 34.09 % compared with Case 2. With the increase of the proportion of biomass gas, the overall trend showed a downward trend.

It can be seen from Fig.3 (b) that compared with the operation and maintenance cost, the operation and maintenance cost of Case 1 increased by 10.8 %～26.76 % compared with Case 2. It can be seen that when the operation and maintenance cost is selected as the target, the maintenance cost and carbon emission are reduced due to the reduction of fuel consumption, and the overall trend is upward.

Table 4 Comparison of Case 1 and Case 2

Natural gas: Biomass gas	1:0	0.75:0.25	0.5:0.5	0.25:0.75	0:1
Carbon emissions/kg	-132.0	-152.2	-96.5	-80.2	-25.6
Operation and maintenance cost/CNY	1235.3	529.5	1110.6	1239.6	1285.7

Corresponding Author E-mail Address: jijie@hyit.edu.cn

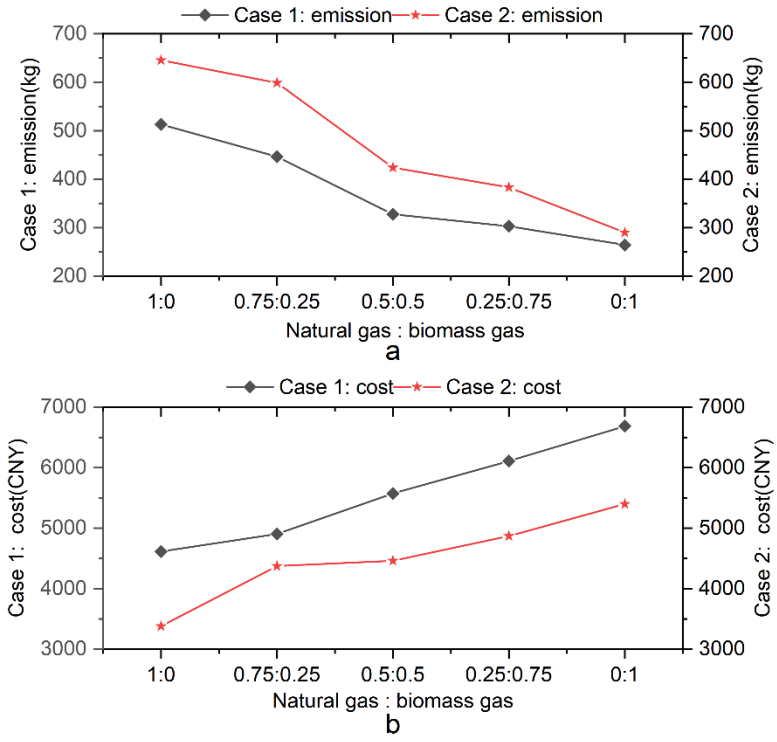

Fig.3 Comparison of Case 1 and Case 2

4.1.2 Comparative Analysis 2

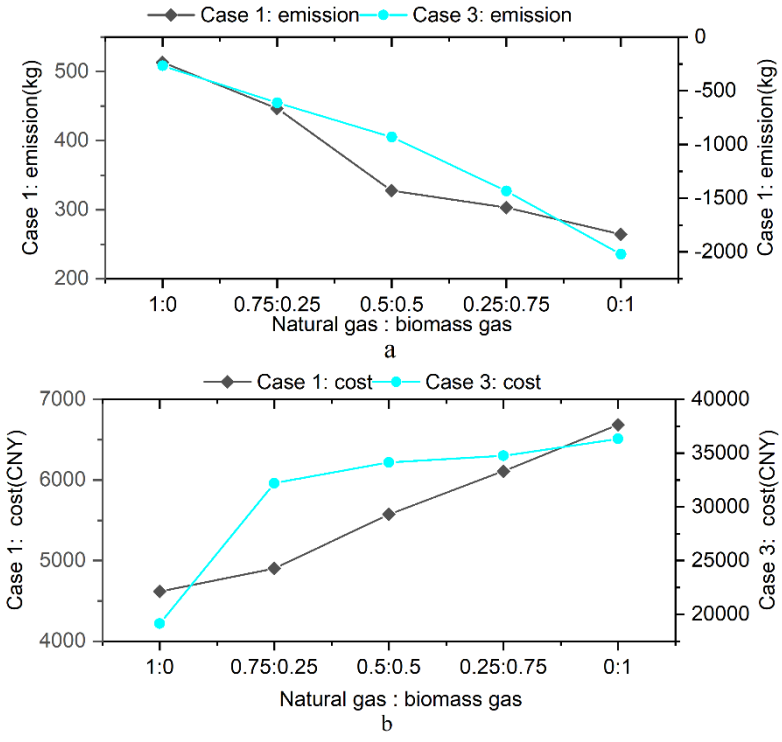

Fig.4 Comparison of Case 1 and Case 3

Corresponding Author E-mail Address: jijie@hyit.edu.cn

From Fig.4 (a) and Table 5, it can be seen that in the case of carbon emissions as a comparison, the carbon emissions generated by the lowest-time Case 1 are 780.1 kg less than Case 3 ; at the highest time, the carbon emissions generated by Case 1 are 2286.3 kg less than Case 3. The difference in carbon emissions between Case 1 and Case 3 is 780.1kg～2286.3kg. As the proportion of biomass gas increases, the gap between the two becomes more and more obvious. It can be seen that in the case of Case 3, each change in the ratio will greatly reduce carbon emissions.

It can be seen from Fig.4 (b) that the negative growth in Case 3 makes the increase of Case 1 increase sharply compared with Case 3. In the case of comparing the operation and maintenance costs between the two, the minimum time Case 1 requires 14514.3 CNY less than the operation and maintenance cost of Case 3; at the highest time, the operation and maintenance cost of Case 1 is 29647.5 CNY less than that of Case 3.

Table 5 Comparison of Case 1 and Case 3

Natural gas: Biomass gas	1:0	0.75:0.25	0.5:0.5	0.25:0.75	0:1
Carbon emissions/kg	780.1	1057.4	1259.1	1737.6	2286.3
Operation and maintenance cost/CNY	14514.3	27298.7	28573.2	28640.9	29647.5

4.1.3 Comparative Analysis 3

From Fig.5 (a) and Table 6, it can be seen that in the case of carbon emissions as a comparison, the carbon emissions generated by Case 2 at the lowest time are 912.08 kg more than Case 3 ; the carbon emissions generated by Case 2 at the highest time are 2311.94 kg more than that of Case 3. Since Case 2 mainly aims at operation and maintenance costs, the fuel cost is reduced, the consumption of natural gas is reduced, and the carbon emissions are reduced.

It can be seen from Fig.5 (b) that as the proportion of biomass gas increases, the operation and maintenance cost shows an upward trend. In the case of comparing the operation and maintenance costs between the two, the minimum time Case 2 requires 15749.6 CNY less than the operation and maintenance costs of Case 3 ; at the highest time, the operation and maintenance cost of Case 2 is 30933.1 CNY less than that of Case 3.

Table 6 Comparison of Case 2 and Case 3

Natural gas: Biomass gas	1:0	0.75:0.25	0.5:0.5	0.25:0.75	0:1
Carbon emissions/kg	912.08	1209.59	1355.61	1817.76	2311.94
Operation and maintenance cost/CNY	15749.6	27828.3	29880.8	29880.5	30933.1

In summary, the carbon emissions and operation and maintenance costs of Case 1 are in a moderate amount, while Case 2 can reduce the operation and maintenance costs well but the carbon emissions will increase to a certain extent. The operation and maintenance costs of Case 3 increase greatly, but the whole system presents a negative emission state. Therefore, the configuration mode of Case 1 is more in line with the low-carbon strategy, while the configuration mode of Case 3 has the possibility of reducing costs and even making profits through carbon trading. The lower the carbon emissions of the entire system in their respective Cases, the higher the operation and maintenance costs.

Corresponding Author E-mail Address: jijie@hyit.edu.cn

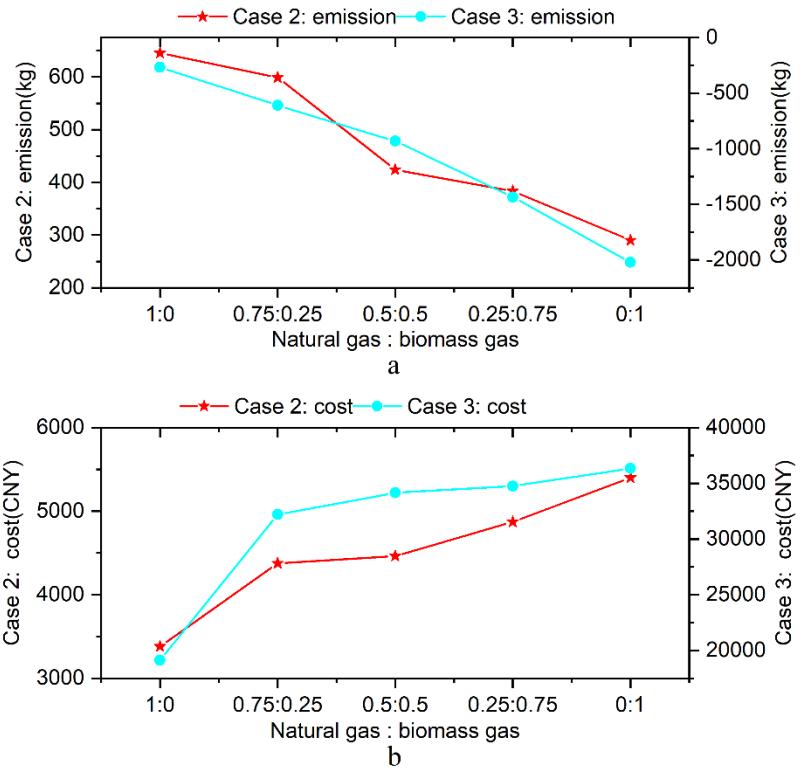

Fig.5 Comparison of Case 2 and Case 3

4.2 Study on the influence of biomass gas ratio

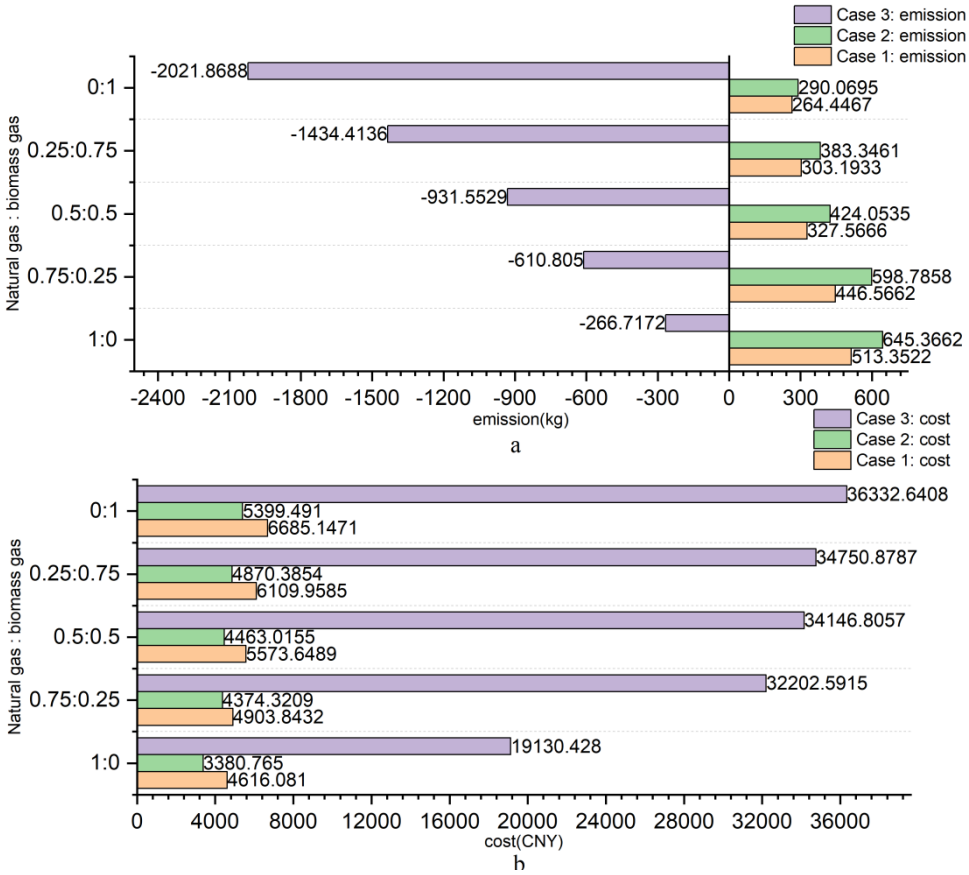

Fig.6 Carbon emissions and operation and maintenance cost data chart

Corresponding Author E-mail Address: jijie@hyit.edu.cn

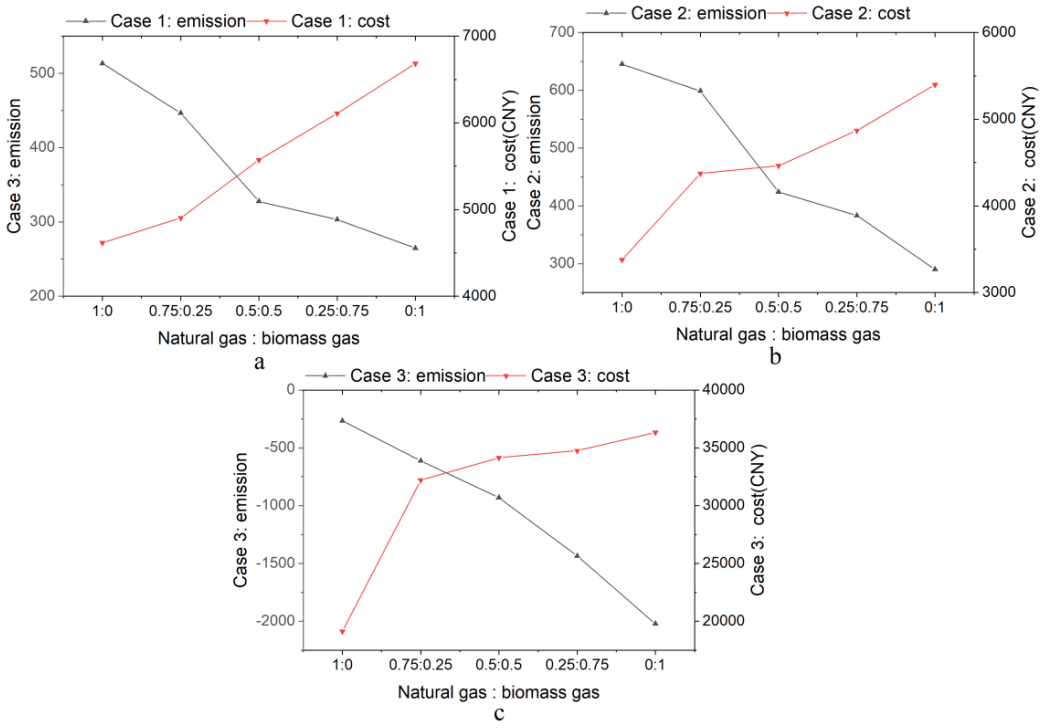

Fig.7 Comparison of the Cases

It can be seen from Fig.6-7 that the carbon emissions decrease with the increase of the proportion of biomass gas, and the operation and maintenance costs increase with the increase of the proportion of biomass gas.

4.3 Research on equipment output characteristics

4.3.1 Electrical balance characteristics under common objectives

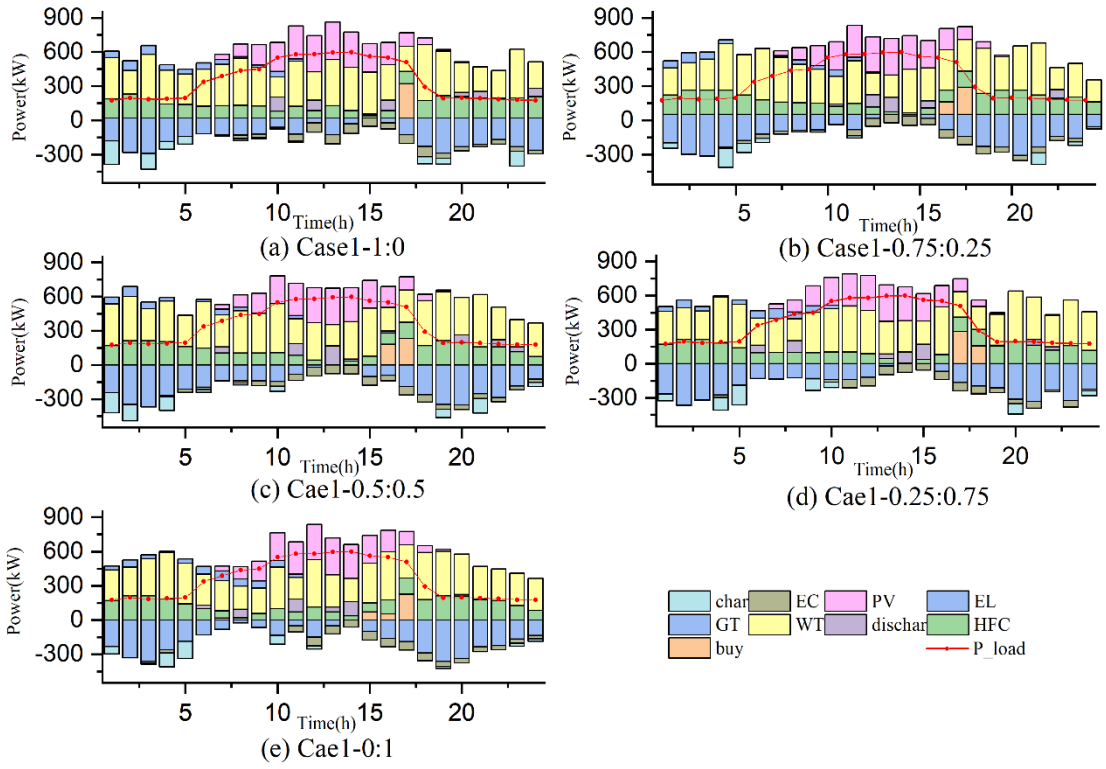

Fig.8 Electric power balance under the common goal

Corresponding Author E-mail Address: jijie@hyit.edu.cn

It can be seen from Fig.8 that the main power supply equipment is wind turbines, photovoltaic units, and hydrogen fuel cells. At 13-16 o 'clock, due to the peak period of electricity consumption, the operating power of the electrolytic hydrogen device is reduced to the lowest to reserve more electricity for electricity load. The power purchase period is mainly between 15-17 o 'clock. The total amount of electricity purchased in Fig.8 (d) is up to 440.99 kW. When the content of biomass gas is high, the maintenance amount of the equipment is also high, so that the power generation is not cost-effective compared to the purchase of electricity, so as to replace the power generation with the purchase of electricity. The results of its operation are shown in table 7 below.

Table 7 Results under the minimum of operation and maintenance cost and carbon emissions

Natural gas: Biomass gas	1:0	0.75:0.25	0.5:0.5	0.25:0.75	0:1
Carbon emissions/kg	513.3	446.6	327.6	303.2	264.4
Operation and maintenance cost/CNY	4616.1	4903.8	5573.7	6109.9	6685.1

4.3.2 Heat balance characteristics under common goals

It can be seen from Fig.9 that the main heating equipment is a hydrogen fuel cell, supplemented by a gas boiler to meet the heat load.1-5 and 18-20 can have excess heat for storage. When the heat is low, the heat load is mainly filled by the heat release of the heat storage tank, thereby reducing the operation of the heating equipment, and its storage capacity can reach up to 138.85 kW · h. The heat converted from the heat exchange device from the gas turbine is almost zero. The heat load generated by the hydrogen fuel cell can be as high as 205.81 kW · h, while the total power is maintained at about 3000 kW. It plays an indispensable role in reducing carbon emissions.

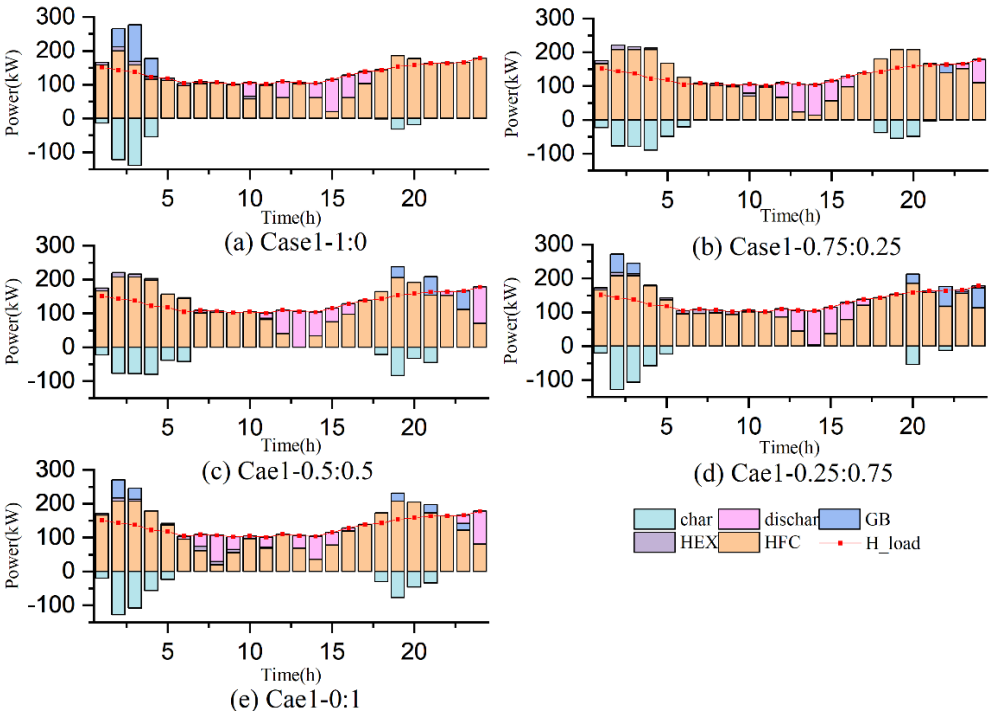

Fig.9 Thermal power balance under common goal

Corresponding Author E-mail Address: jijie@hyit.edu.cn

4.3.3 Cold balance characteristics under common goals

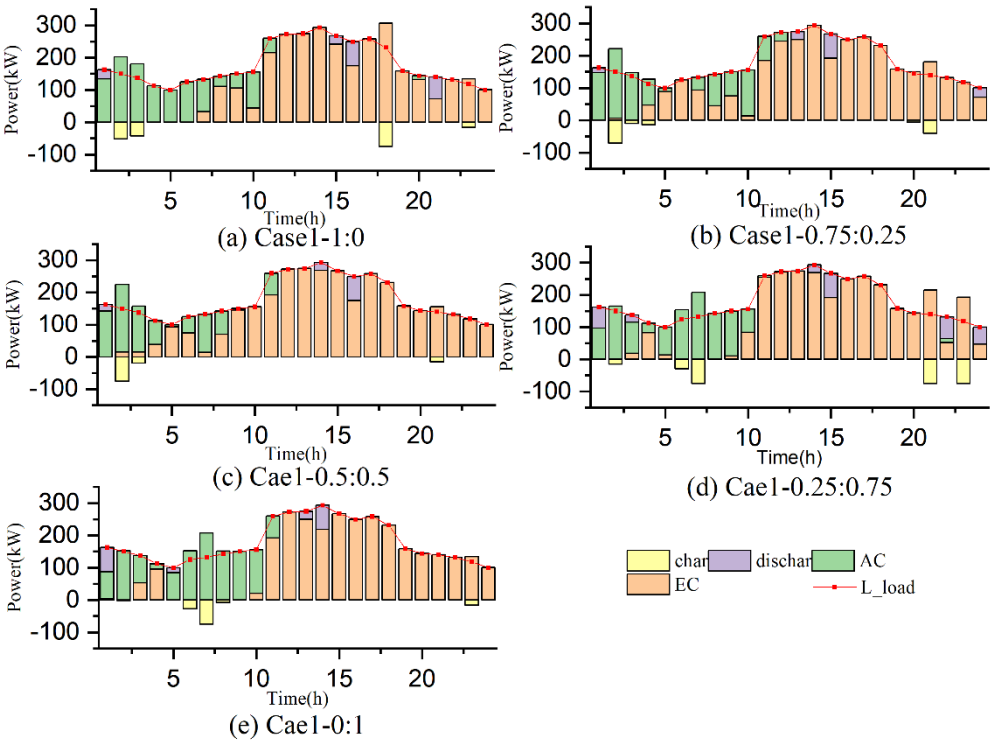

Fig.10 Cooling power balance under common goal

It can be seen from Fig.10 that the main cooling equipment is lithium bromide chiller and electric refrigerator. When the cooling load demand is low at 1-10, the heat load generated by the gas turbine can be converted from lithium bromide chiller to cooling load. The converted cooling load is as high as that of the electric refrigerator at the peak of the cooling load demand. The average total power of the electric refrigerator at each ratio is 3112.17 kW.

4.3.4 Electrical balance characteristics under operation and maintenance objectives

It can be seen from Fig.11 and Table 8 that the main power supply equipment is wind turbine, photovoltaic unit and hydrogen fuel cell. At 13-16 o 'clock, due to the peak period of electricity consumption, the operating power of the electrolytic hydrogen device is reduced to the minimum, so as to reserve more electricity to supply the electricity load. The total operating power is maintained at about 4350 kW, indicating that it plays a huge role in reducing carbon emissions, and mainly at the time of low demand for electricity load, the electrolytic hydrogen device will gradually operate at full capacity. The power purchase period is mainly between 16: 00-18: 00, and the maximum power purchase in Fig.6(b) is 555.44 kW · hat this time, the strong operation of the electrolytic hydrogen equipment and the high demand of the electric load make the system need to purchase power. The general operating output is similar to Case 1. The results of its operation are shown in table 2 below.

Table 8 The results under the operation and maintenance cost target

Natural gas: Biomass gas	1:0	0.75:0.25	0.5:0.5	0.25:0.75	0:1
Carbon emissions/kg	645.3662	598.7858	424.0535	383.3461	290.0695
Operation and maintenance cost/CNY	3380.765	4374.3209	4463.0155	4870.3854	5399.491

Corresponding Author E-mail Address: jijie@hyit.edu.cn

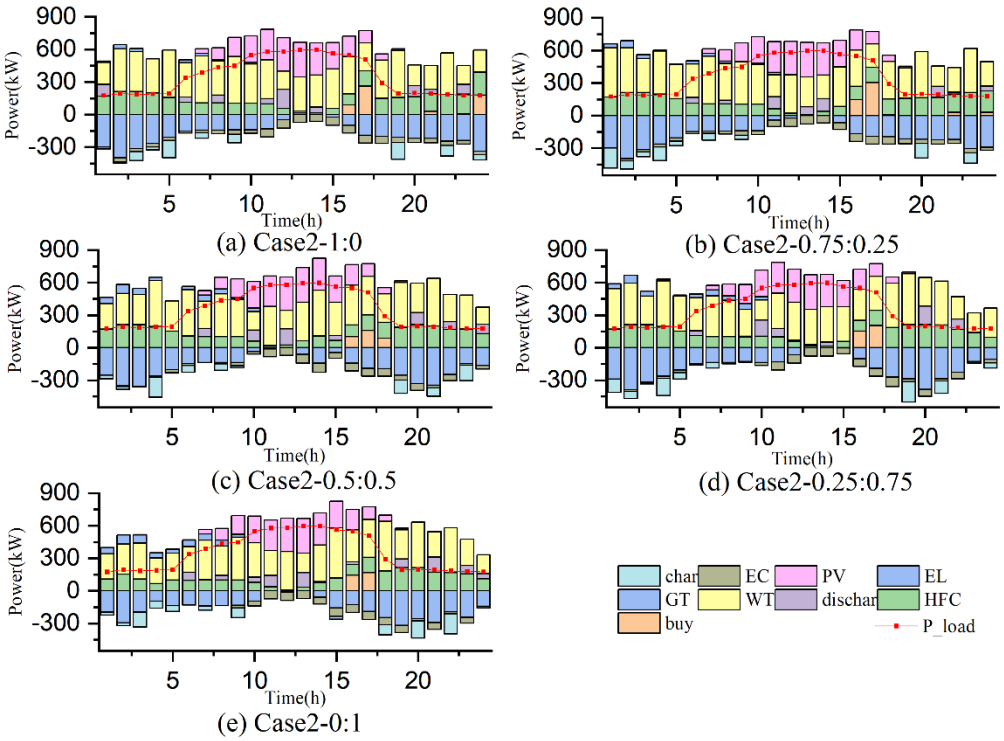

Fig.11 Electric power balance under operation and maintenance target

4.3.5 Heat balance characteristics under operation and maintenance objectives

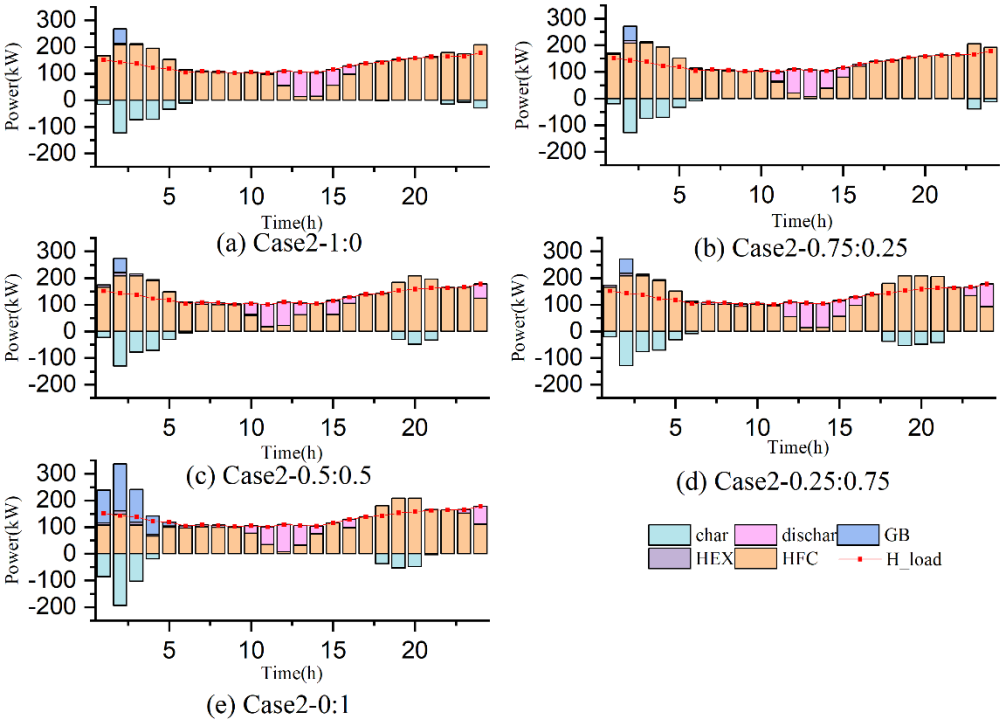

Fig.12 Thermal power balance under operation and maintenance target

It can be seen from Fig.12 that the main heating equipment is a hydrogen fuel cell, and the gas boiler is used as a supplement to meet the heat load. On the whole, as long as the gas boiler outputs, it will lead to a significant increase in the heat reserves at that time. In Fig.10 (e) 1-4, the

Corresponding Author E-mail Address: jijie@hyit.edu.cn

gas boiler greatly provides heat, and its power can reach 176.77 kW ·h. At the same time, its thermal storage capacity reaches 194.17 kW ·h, which provides great convenience for subsequent thermal scheduling. In addition to the total supply of hydrogen fuel cells at Fig.10 (a) is 2683.15 kW, the total supply is maintained at 3100 kW at other ratios, indicating that hydrogen fuel cells contribute greatly to the reduction of carbon emissions. The heat converted from the heat exchange device at the gas turbine is almost zero. The general operating output is similar to Case 1.

4.3.6 Cold balance characteristics under operation and maintenance objectives

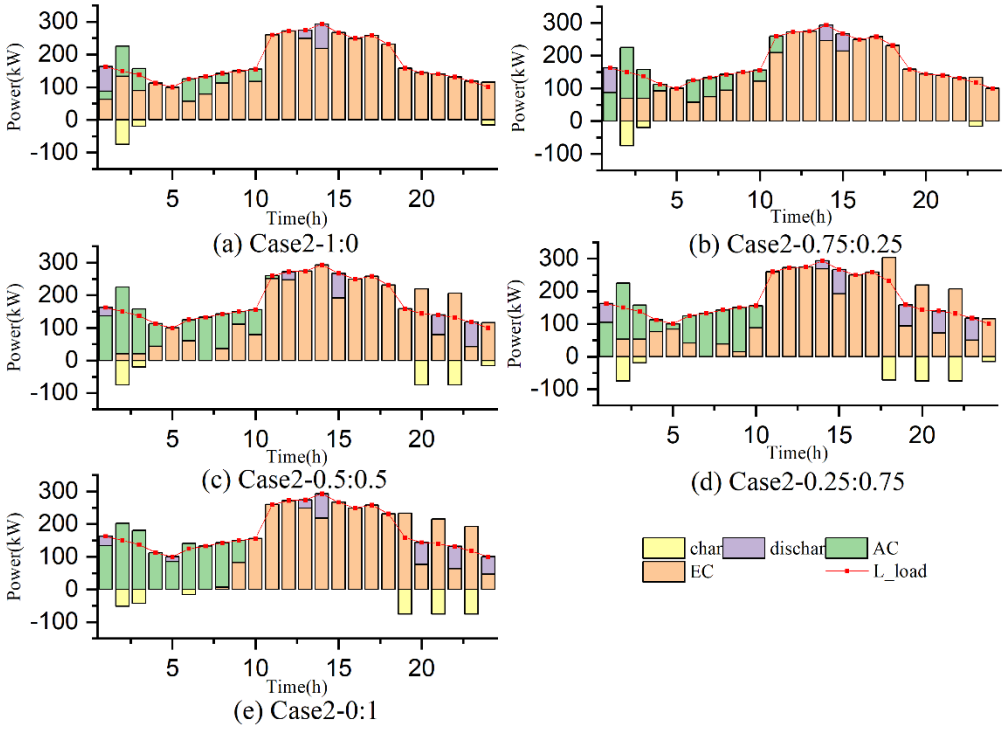

Fig.13 Cold power balance under operation and maintenance target

It can be seen from Fig.13 that the main cooling equipment is lithium bromide chiller and electric refrigerator. With the increase of the proportion of biomass gas, the output of lithium bromide chiller is increasing, and the electric refrigerator is still the main source of cooling. The average total power of the electric refrigerator at each ratio is 3412.71 kW, which is 9.66 % higher than Case 1.

4.3.7 Electrical balance characteristics under carbon emission targets

It can be seen from Fig.14 and Table 9 that no external power purchase is required under each ratio. Therefore, it can be found that the relationship between carbon emissions leads to the existence of electricity purchase in the first two optimization objectives. In (a), due to the fact that it is all-natural gas, the electrolytic hydrogen device operates for 24 hours to reduce carbon emissions, and the hydrogen fuel cell also operates for 24 hours to reduce carbon emissions. In the overall proportion, as the proportion of natural gas decreases, the hydrogen fuel cell gradually no longer operates. The average operating power of the electrolytic hydrogen device is 3764.01 kW, and the highest in (a) can reach 5560.1 kW.

In the case of carbon emissions as the goal, the electrolytic hydrogen device works uninterruptedly to produce hydrogen, and then the methane generator absorbs carbon dioxide in the atmosphere, showing a negative emission state. The operation and maintenance costs and

Corresponding Author E-mail Address: jijie@hyit.edu.cn

carbon emissions under each ratio are shown in Table 3.

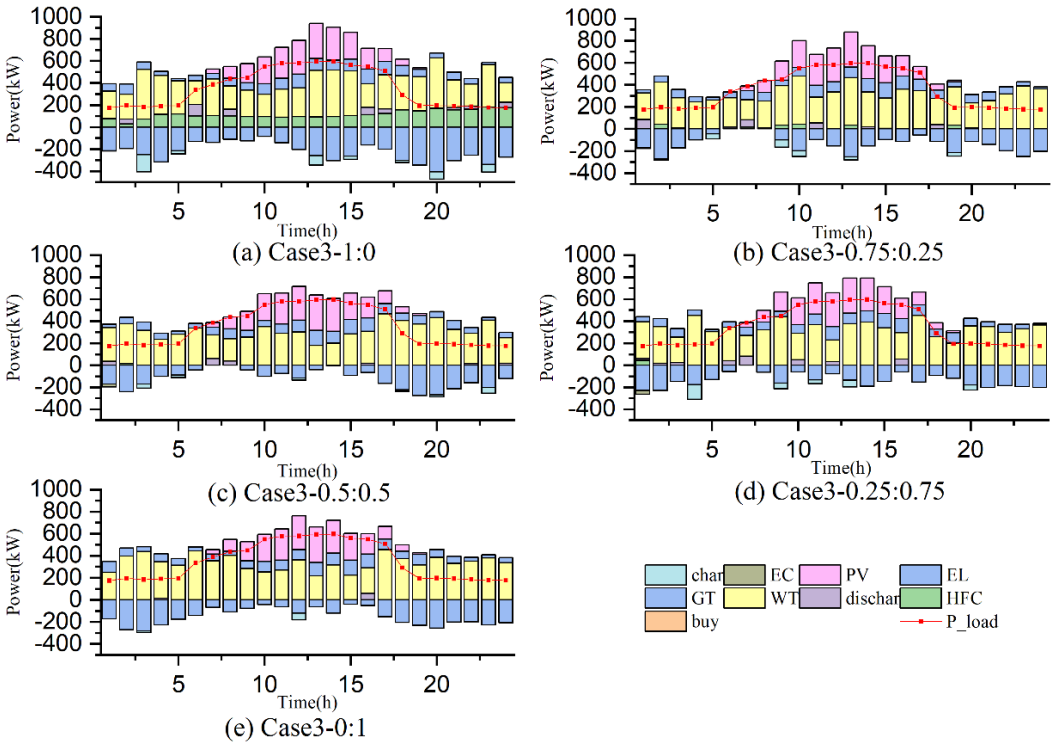

Fig.14 Electric power balance under carbon emission target

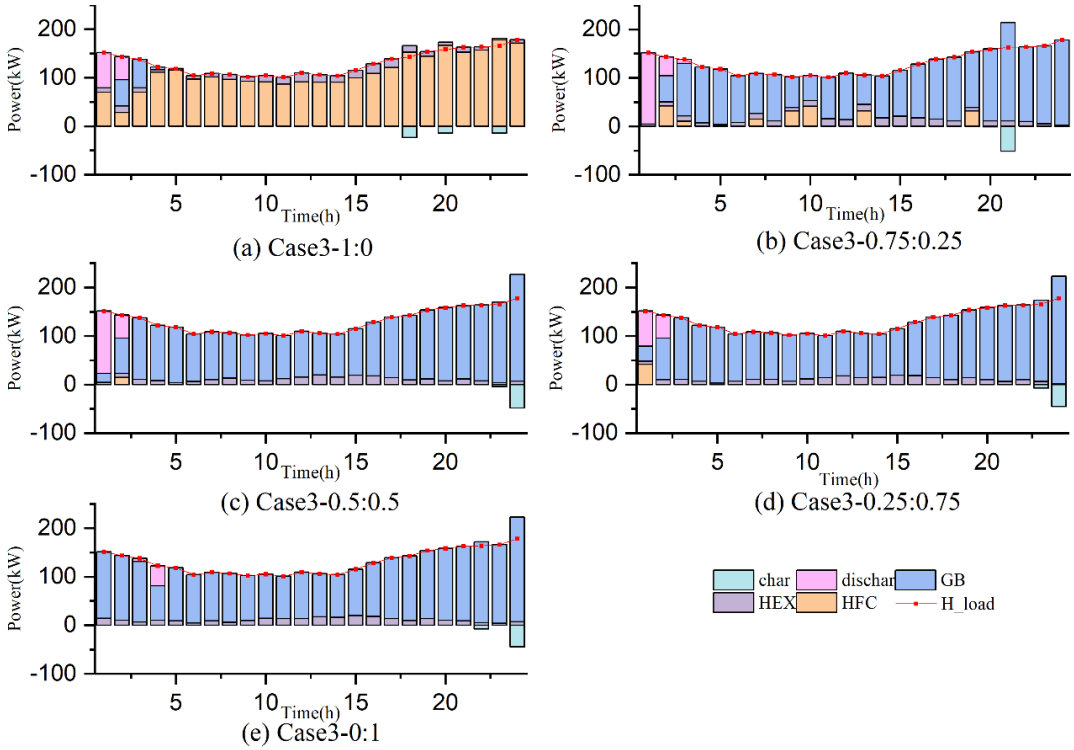

Fig.15 Thermal power balance under carbon emission target

4.3.8 Heat balance characteristics under carbon emission targets

It can be seen from Fig.15 (a) that the hydrogen fuel cell is mainly used for comprehensive heating, and the maximum operating power is 177.66 kW. At other ratios, the hydrogen fuel cell is maintained at a lower power, while the gas boiler is fully supplied by the fuel boiler due to the

Corresponding Author E-mail Address: jijie@hyit.edu.cn

presence of the hydrogen fuel cell and the carbon emissions are absorbed, and its maximum operating power can reach 221.16 kW. Under the carbon emission target, the carbon emissions generated by the fuel boiler are absorbed and utilized by the system, so that the fuel cell, a highly efficient heat production equipment, is heated by the equipment with the same high carbon emissions.

Table 9 Results under carbon emission targets

Natural gas: Biomass gas	1:0	0.75:0.25	0.5:0.5	0.25:0.75	0:1
Carbon emissions/kg	-266.7172	-610.805	-931.5529	-1434.4136	-2021.8688
Operation and maintenance cost/CNY	19130.428	32202.5915	34146.8057	34750.8787	36332.6408

4.3.9 Cold balance characteristics under carbon emission targets

It can be seen from Fig.16 that the overall supply is from the lithium bromide chiller, and its maximum operating power can reach 338.6 kW. It is also because of the vigorous operation of electrolytic hydrogen, the high-power operating gas turbine makes the lithium bromide chiller supply a lot of cold. The electric refrigerator will also provide some help at time 0.

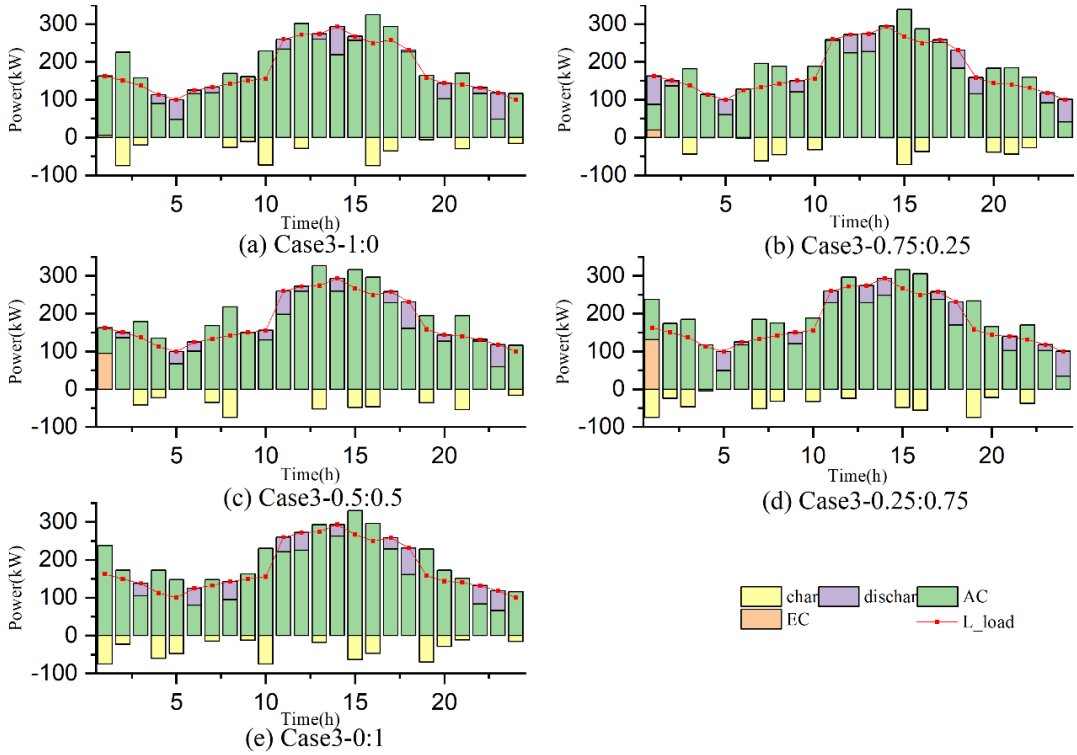

Fig.16 Cold power balance under carbon emission target

4.4 Model validation

In this paper, a CCHP system based on the influence of different optimization objectives under the co-combustion of natural gas and biomass gas is constructed by MATLAB, and added to the original system model. The influence of different biomass mixing ratios and different optimization objectives is mainly introduced. The establishment of the energy storage model is slightly rough, and the reliability of the structure is verified by the reference model. Its efficiency is shown in Table 10, and its operation and maintenance efficiency are shown in Table 11.

Corresponding Author E-mail Address: jijie@hyit.edu.cn

Table 10 Efficiency model validation

Equipment	Work efficiency	Reference [36]	Error
GT	0.35	/	/
GB	0.9	0.95	0.06%
EL	0.87	0.87	/
MR	0.6	0.6	/
HFC	0.85	0.95	0.12%
EC	4	5.3	0.24%
AC. W	1.31	1.31	/

Table 11 Operation and maintenance efficiency verification

Equipment	Operating efficiency	Reference [29, 38]	Error
GT	0.05CNY/kWh	0.03CNY/kWh	0.4%
GB	0.35CNY/kWh	0.355CNY/kWh	0.1%
P2G	0.15CNY/kWh	0.2CNY/kWh	0.25%
EC	0.0004CNY/MJ	0.0005CNY/MJ	0.2%
AC. W	0.0002 CNY /MJ	0.0002 CNY /MJ	/

The results show that the output simulation of the system under various working conditions has high accuracy. Therefore, the scheduling optimization research based on this model has practical significance and can guide the comprehensive evaluation of the system and subsequent design improvement.

4.5 Sensitivity Analysis

Table 12 Data Sensitivity Analysis**.**

Natural gas: Biomass gas	Carbon emissions/kg	Range of Change/%	Operation and maintenance cost/CNY	Range of Change/%
100:0	513.3522	/	4616.081	/
90:10	488.6140	4.8%	4821.8340	-4.5%
80:20	463.3528	4.9%	5026.9785	-4.4%
70:30	437.8882	5.0%	5233.1549	-4.5%
60:40	413.1959	4.8%	5438.3494	-4.4%
50:50	388.4345	4.8%	5643.5696	-4.4%
40:60	363.9297	4.8%	5848.5941	-4.4%
30:70	338.8317	4.9%	6053.7595	-4.4%
20:80	313.4919	4.9%	6260.5535	-4.5%
10:90	288.7703	4.8%	6467.1751	-4.5%
0:100	264.4467	4.7%	6685.1471	-4.7%

In this study, a sensitivity analysis was conducted on a single variable - the proportion of biomass gas - to observe its impact on carbon emissions and operation and maintenance (O&M) costs.

As the proportion of biomass gas increases from 0% to 100%, carbon emissions gradually decrease. This is because biomass is generally considered more environmentally friendly than natural gas, resulting in lower carbon emissions from its combustion. The percentage decrease in carbon emissions ranges from 4.7% to 4.9%, indicating a significant impact of the introduction of biomass gas on reducing carbon emissions.

Contrary to the trend of carbon emissions, O&M costs gradually increase with the increasing

Corresponding Author E-mail Address: jijie@hyit.edu.cn

proportion of biomass gas. This may be due to higher costs associated with the processing, storage, and transportation of biomass gas, or higher maintenance costs for biomass gas combustion equipment. The percentage increase in O&M costs ranges from 4.4% to 4.7%. This suggests that as the proportion of biomass gas increases, O&M costs also gradually rise.

Therefore, from the perspective of reducing carbon emissions, increasing the proportion of biomass gas usage is beneficial. Biomass gas can serve as an alternative energy source for mitigating greenhouse gas emissions. However, from the perspective of O&M costs, increasing the proportion of biomass gas usage may lead to increased costs. This requires careful consideration and balancing when making decisions to determine the optimal energy mix ratio.

5 Conclusions

In this study, a SIGE-CCHP system was developed to investigate the intricate coupling challenges associated with integrating biomass gas and natural gas within a Combined Cooling, Heating, and Power (CCHP) framework. The comprehensive analysis of the system's operational performance across diverse optimization objectives yielded several significant scientific discoveries and practical applications.

1) An increase in the proportion of biomass gas was observed to gradually decrease the system's carbon emissions, albeit with a concurrent rise in operational and maintenance costs. This finding establishes a theoretical basis for the blended utilization of biomass energy and natural gas, providing valuable insights for future energy system design and operational management.

2) Optimization for operational and maintenance costs was shown to yield optimal system performance, with a mixing ratio of 1:1 between biomass gas and natural gas minimizing carbon emissions while significantly reducing costs. This discovery offers crucial practical guidance for the mixed combustion of these gases, promoting efficient and environmentally friendly energy system operations.

3) When optimizing for carbon emissions, the study revealed that the system can transform into a carbon sequestration system, achieving a maximum absorption capacity of up to 2021.86kg. This capability effectively sequesters carbon dioxide from the atmosphere, offering novel ideas and methods for carbon emission reduction and sequestration, with profound implications for environmental protection.

4)During the optimization of operational and maintenance costs, it was observed that carbon emissions increased by 9.69% to 34.09% compared to concurrent optimization of both objectives. Conversely, operation and maintenance costs decreased by 10.8% to 26.76%. This trade-off underscores the intricate balancing act required in energy system optimization, highlighting the need for a comprehensive approach that considers both environmental and economic impacts.

In conclusion, this study provides valuable insights into the integration of biomass gas and natural gas within a CCHP system, offering both theoretical and practical guidance for energy system design, operational management, and carbon emission reduction. The findings have profound implications for promoting efficient and environmentally friendly energy system operations, contributing to the sustainable development of energy systems.

Follow-up research can consider the use of pure clean energy as input and reduce their own operation and maintenance costs, the use of carbon absorption system for the reduction of various carbon emissions or through carbon trading to obtain funds for their own profitability; considering that the instability of wind power will also have a great impact on the system, the uncertain output of new energy can be studied in the future.

Corresponding Author E-mail Address: jijie@hyit.edu.cn

Data availability statement:

The data used to support the findings of this study were supplied by Zitong Lin under license and so cannot be made readily available. Requests for access to these data should be made to the corresponding author.

Reference

[1] XIONG J, PENG T, TAO Z, et al. A dual-scale deep learning model based on ELM-BiLSTM and improved reptile search algorithm for wind power prediction [J]. Energy, 2023, 266: 126419.

[2] ZHANG X, LIU X, SUN X, et al. Thermodynamic and economic assessment of a novel CCHP integrated system taking biomass, natural gas and geothermal energy as co-feeds [J]. Energy Conversion and Management, 2018, 172: 105-18.

[3] ZHANG L, ZHANG L, SUN B, et al. Nested optimization design for combined cooling, heating, and power system coupled with solar and biomass energy [J]. International Journal of Electrical Power & Energy Systems, 2020, 123.

[4] ZHU P, WU Z, GUO L, et al. Achieving high-efficiency conversion and poly-generation of cooling, heating, and power based on biomass-fueled SOFC hybrid system: Performance assessment and multi-objective optimization [J]. Energy Conversion and Management, 2021, 240.

[5] ANVARI S, SZLĘK A, ARTECONI A, et al. Comparative study of steam injection modes for a proposed biomass-driven cogeneration cycle: Performance improvement and CO2 emission reduction [J]. Applied Energy, 2023, 329.

[6] EBRAHIMI-MOGHADAM A, FARZANEH-GORD M. A sustainable optimal biomass waste-driven CCHP system to boost the nearly zero energy building concept [J]. Energy Conversion and Management, 2023, 277.

[7] LI H, BIN KALEEM M, LIU Z, et al. IoB: Internet-of-batteries for electric Vehicles–Architectures, opportunities, and challenges [J]. Green Energy and Intelligent Transportation, 2023, 2(6): 100128.

[8] LI H, KALEEM M B, CHIU I-J, et al. An intelligent digital twin model for the battery management systems of electric vehicles [J]. International Journal of Green Energy, 2023.

[9] CHANG L, WU Z, GHADIMI N. A new biomass-based hybrid energy system integrated with a flue gas condensation process and energy storage option: An effort to mitigate environmental hazards [J]. Process Safety and Environmental Protection, 2023, 177: 959-75.

[10] WEGENER M, MALMQUIST A, ISALGUE A, et al. A techno-economic optimization model of a biomass-based CCHP/heat pump system under evolving climate conditions [J]. Energy Conversion and Management, 2020, 223.

[11] RAJABI HAMEDANI S, VILLARINI M, MARCANTONIO V, et al. Comparative energy and environmental analysis of different small-scale biomass-fueled CCHP systems [J]. Energy, 2023, 263.

[12] ZHANG D, ZHANG B, ZHENG Y, et al. Economic assessment and regional adaptability analysis of CCHP system coupled with biomass-gas based on year-round performance [J]. Sustainable Energy Technologies and Assessments, 2021, 45.

[13] WANG Z X, LI H Y, ZHANG X F, et al. Performance analysis on a novel micro-scale combined cooling, heating and power (CCHP) system for domestic utilization driven by biomass energy [J]. Renewable Energy, 2020, 156: 1215-32.

[14] DIYOKE C, NGWAKA U, ONAH T O. Comparative assessment of a hybrid of gas turbine and

Corresponding Author E-mail Address: jijie@hyit.edu.cn

biomass power system for sustainable multi-generation in Nigeria [J]. Scientific African, 2021, 13.

[15] JIE P, LI Z, REN Y, et al. Economy-energy-environment optimization of biomass gasification CCHP system integrated with ground source heat pump [J]. Energy, 2023, 277.

[16] YANG S, PENG S, XIAO Z, et al. Energetic and exergetic analysis of a biomass-fueled CCHP system integrated with proton exchange membrane fuel cell [J]. International Journal of Hydrogen Energy, 2023, 48(36): 13603-16.

[17] WANG J, CUI Z, YAO W, et al. Regulation strategies and thermodynamic analysis of combined cooling, heating, and power system integrated with biomass gasification and solid oxide fuel cell [J]. Energy, 2023, 266.

[18] WANG S, CHEN X, WEI B, et al. Thermodynamic analysis of a net zero emission system with CCHP and green DME production by integrating biomass gasification [J]. Energy, 2023, 273.

[19] YANG Z, JINGCHUN W U, ELMASRY Y, et al. Techno-economic and multi objective optimization of zero carbon emission biomass based supercritical carbon dioxide oxy combustion system integrated with carbon dioxide liquefaction system and solid oxide electrolyzer [J]. Journal of CO2 Utilization, 2022, 64.

[20] HAO Q, ZHU L, WANG Y, et al. Achieving near-zero emission and high-efficient combined cooling, heating and power based on biomass gasification coupled with SOFC hybrid system [J]. Fuel, 2024, 357.

[21] LI S, ZHU L, HE Y, et al. Thermodynamic evaluation of CCHP system based on biomass gasification by exploring the feasibility of using CO2 as gasification agent [J]. Sustainable Energy Technologies and Assessments, 2020, 42.

[22] MORADI R, CIOCCOLANTI L, DEL ZOTTO L, et al. Comparative sensitivity analysis of micro-scale gas turbine and supercritical CO2 systems with bottoming organic Rankine cycles fed by the biomass gasification for decentralized trigeneration [J]. Energy, 2023, 266.

[23] LI X, KAN X, SUN X, et al. Performance analysis of a biomass gasification-based CCHP system integrated with variable-effect LiBr-H2O absorption cooling and desiccant dehumidification [J]. Energy, 2019, 176: 961-79.

[24] PERRONE D, CASTIGLIONE T, MORRONE P, et al. Numerical and experimental assessment of a micro-combined cooling, heating, and power (CCHP) system based on biomass gasification [J]. Applied Thermal Engineering, 2023, 219.

[25] CHEN J, LI X, DAI Y, et al. Energetic, economic, and environmental assessment of a Stirling engine based gasification CCHP system [J]. Applied Energy, 2021, 281.

[26] JALILI M, GHASEMPOUR R, AHMADI M H, et al. An integrated CCHP system based on biomass and natural gas co-firing: Exergetic and thermo-economic assessments in the framework of energy nexus [J]. Energy Nexus, 2022, 5.

[27] ZHANG X, ZENG R, MU K, et al. Exergetic and exergoeconomic evaluation of co-firing biomass gas with natural gas in CCHP system integrated with ground source heat pump [J]. Energy Conversion and Management, 2019, 180: 622-40.

[28] YANG K, ZHU N, DING Y, et al. Exergy and exergoeconomic analyses of a combined cooling, heating, and power (CCHP) system based on dual-fuel of biomass and natural gas [J]. Journal of Cleaner Production, 2019, 206: 893-906.

[29] Yongli Wang, Hao Xiang, Shuqing Li. Operation optimization of regional integrated energy system considering coupling characteristics of CCHP system [J]. Science Technology and

Corresponding Author E-mail Address: jijie@hyit.edu.cn

Engineering, 2023, 23(18): 7787-97.

[30] Jidong Wang, Yinan Bian, Qiuming Xu. et al. Distributed robust optimal scheduling of microgrid considering risk and carbon trading mechanism [J]. High Voltage Technique,2023, 1-12.

[31] Yan Deng, Zan Gong, Likang Wu. et al. Optimization of cooling heating power system based on complementary characteristics of equipment [J]. Acta Energies Solaris Sinica, 2023, 44(07): 88-95.

[32] KESKIN I, SOYKAN G. Distribution grid electrical performance and emission analysis of combined cooling, heating and power (CCHP)-photovoltaic (PV)-based data center and residential customers [J]. Journal of Cleaner Production, 2023, 414: 137448.

[33] SIQIN Z, NIU D, WANG X, et al. A two-stage distributionally robust optimization model for P2G-CCHP microgrid considering uncertainty and carbon emission [J]. Energy, 2022, 260: 124796.

[34] YOUSEFI H, GHODUSINEJAD M H, NOOROLLAHI Y. GA/AHP-based optimal design of a hybrid CCHP system considering economy, energy and emission [J]. Energy and Buildings, 2017, 138: 309-17.

[35] MOHAMMADKHANI N, SEDIGHIZADEH M, ESMAILI M. Energy and emission management of CCHPs with electric and thermal energy storage and electric vehicle [J]. Thermal Science and Engineering Progress, 2018, 8: 494-508.

[36] Jinpeng Chen, Zhijian Hu, Yingguang Chen, et al. Thermoelectric optimization of integrated energy system considering stepped carbon trading mechanism and electric hydrogen production [J]. Power System Automation Equipment, 2021, 41(09): 48-55.

[37] JIE J, JINGXIN Q, RUNDONG J, et al. Study of energy scheduling and optimal cost management of a new structure CCHP system: A case study supplying energy for a chemical enterprise in Jiangsu Province %J Energy Reports [J]. 2022, 8: 14499-515.

[38] Zhe Bao, Wei Li, Xiaofang Zhang. et al. Research on robust chance constrained optimization of multi-energy cogeneration system based on wind and light joint output simulation [J]. Acta Simulata Systematica Sinica,2023, 1-18.

Corresponding Author E-mail Address: jijie@hyit.edu.cn